İSTANBUL UNIVERSITY CERRAHPAŞA

ORIGINAL ARTICLE
Electrica 2023; 23(2): 345-356

Real-Time Validation of Two-Generator-Based Isolated Hybrid Microgrid System Using a Nine-Switch Converter

Abhijeet Choudhury[1], Swagat Pati[1], Renu Sharma[2], Sanjeeb Kumar Kar[1]

[1]Department of Electrical Engineering, ITER, Siksha O Anusandhan Deemed to be University, Bhubaneswar, Odisha, India
[2]Department of Electrical Engineering, Siksha O Anusandhan Deemed to be University, Bhubaneswar, Odisha, India.

Cite this article as: A. Choudhury, S. Pati, R. Sharma and S. Kumar Kar, "Real-time validation of two-generator-based isolated hybrid microgrid system using a nine-switch converter," *Electrica*, 23(2), 345-356, 2023.

ABSTRACT

In this paper, in order to configure a hybrid microgrid system (HMS), a topological representation for nine-switch converters (NSCs) has been introduced to interface multiple renewable power generation systems. Here, a 22 kW self-excited induction generator is interfaced with a 7.5 kW doubly fed induction generator using an NSC. The active power flow in the system has been managed by a battery energy storage system connected at the Direct current (DC) link of the NSC. The grid-side converter of the Doubly-fed Induction Generator (DFIG)-based wind energy conversion system (WECS) manages the reactive power flow of the system. Moreover, the NSC helps in managing both the stator-side and the rotor-side power flow of the DFIG-based WECS. This proposed system is subjected to different time-varying loads, and the execution of the structure has been examined. This proposed system is simulated and modeled utilizing MATLAB/Simulink and verified using OPAL-RT 4510.
***Index Terms*—**Back converter, battery energy storage, grid flux-oriented vector control, hybrid microgrid system, nine-switch converter, stator flux-oriented vector control, wind energy conversion system.

I. INTRODUCTION

In this modernizing scenario, the energy crisis has reached its peak considering the depletion of conventional energy sources. Customers are frequently facing blackouts in rural as well as urban areas. In order to mitigate these issues, renewable power generation (RPGs) has been taken into consideration both in isolated and in grid-connected modes of operation. Regarding RPG, the focus remains on wind, Photovoltaic (PV), and micro-hydro generation. Now if a single RPG is considered without any energy storage device, then it is quite similar to the conventional system. Hence, researchers have been smart enough in hybridizing multiple numbers of RPGs for reliable and efficient power supply. The hybridization or integration of energy sources is possible only by means of power electronic converters. Out of various types of power converters, back-to-back (BTB) converters have been precisely used for RPG systems. It has come to the notice that when multiple RPGs are integrated, BTB converters play a vital role to form a grid-connected system or an isolated microgrid system.

Apart from integration, these BTB converters can also be seen for applications oriented to high-voltage DC transmission systems. These converters provide an extraordinary independent control, where multiple parameters can be controlled independently, and this is possible due to the presence of a DC link. Back-to-back converters are usually seen in wind-power applications, at which two- and six-switch converters (SSCs) are connected back to back. One acts as the grid-side converter (GSC) and the other acts as the machine-side converter (MSC). Both the control algorithms are different in order to control the parameters independently. Moreover, the speed of the wind generator is taken care of by the MSC and the power flow of the wind energy conversion system (WECS) is taken care of by the GSC as given in [1]. The BTB converters help in controlling the power flow with precise compensated voltage as well as current around a unified power flow controller as studied in [2]. In [3, 4], a hybrid microgrid system (HMS) has been considered which comprises a squirrel cage induction generator-based WECS using BTB converters, interfaced with a micro-hydro system housing an SEIG. A battery energy storage (BES) is attached across the DC link of an HMS, in order to supply/store deficit/excess amount of active power. The power flow

Corresponding author:
Swagat Pati

E-mail:
swagatiter@gmail.com

Received: September 27, 2022

Accepted: November 24, 2022

Publication Date: March 30, 2023

DOI: 10.5152/electrica.2023.220174

using BTB converters for doubly fed Induction generator (IG)-based WECS is delineated in [5], which gives a profound knowledge on the vector control of both the converters separately. A novel stator flux-oriented vector control (SFOVC) approach has been accustomed to control the RSC as given in [6] along with grid voltage-oriented vector control is utilized for GSC is given in [7].

Using two SSCs connected back to back houses 12 number of switches; hence researchers thought of reducing the number of switches in order to enhance the cost of converter. Many literatures have been proposed about the matrix converter as well as nine-switch converters (NSCs) for power control and integration of RPGs. Though a matrix converter poses nine bidirectional switches, the absence of DC link does not make it fruitful for controlling the power flow independently. But in the case of NSCs, the converter possesses nine bidirectional switches along with the presence of a DC link. Furthermore, a decoupled/independent power control can be easily achieved in the case of NSCs. [8] enhances the utility of two AC loads connected across the terminals of NSC which is supplied from a single DC source. In [9], NSC acts as an interfacing unit for a WECS and the conventional grid. The power control of two different sources of energy supplying power to the conventional grid is delineated in [10]. Two different frequency mode of operation of NSC is suggested by the authors in [11]. The utilization of a coupling transformer and a DC–DC converter can be readily replaced by an NSC. Essentially, each phase leg of an NSC includes three bidirectional switches. It has the capacity to power two AC systems at various voltages and frequencies. In contrast to BTB converters, these NSCs are more dependable and effective. But compared to a BTB converter as shown in [12], a larger DC link voltage is needed with NSC. The entire switching scheme, control strategy, and the mathematical modeling for NSC are given in [13-15]. Researchers in [16] have incorporated PV-SEIG using NSCs to confirm the continuous power supply across the system regardless of load and source side change.

In this work, an isolated microgrid system has been proposed, which includes a 22 kW micro-hydro system housing an SEIG and a WECS housing a 7.5 kW DFIG. The NSC behaves as an interface that links the micro-hydro system and WECS. A BES is attached at the DC link of the NSC, which helps in conserving or releasing excess/deficit power during power supply. Primarily, this HMS is subjected to different loads like base Resistance-Inductive (RL) load, rectifier load, and induction motor load. The performance of the entire system is studied by subjecting it to time-varying loads. The modeling and simulation of the proposed work have been done in the Matrix Laboratory platform and verified using OPAL-RT simulator (OP-4510).

II. SYSTEM DESCRIPTION

In this proposed work, a constant power source-based SEIG system [17] is interfaced with a DFIG impelled by a wind generator given [18] and [19]. Though the operation of DFIG stimulates both MSCs and GSCs, here both these converters are replaced by a single NSC.

Here the NSC controls the wind side power flow as well as compensates for both real and reactive power demand to/from the system. The simultaneous approach of NSC helps the system's frequency and voltage to be maintained at a steady tolerance limit. Moreover, a battery bank is connected at the DC link of the NSC, which helps in storing or supplying power as per the requirement in/from the system. This isolated HMS is applied to three distinct time-varying loads namely a conventional RL load, rectifier load, and induction motor load. With the variable or step change in both the torques of SEIG and DFIG, the power flow of the entire system is analyzed using an NSC. The entire control structure and system diagram of this HMS is given in Fig. 1. The system is modeled and simulated using Simulink/MATLAB environment and is verified using OPAL-RT 4510 series.

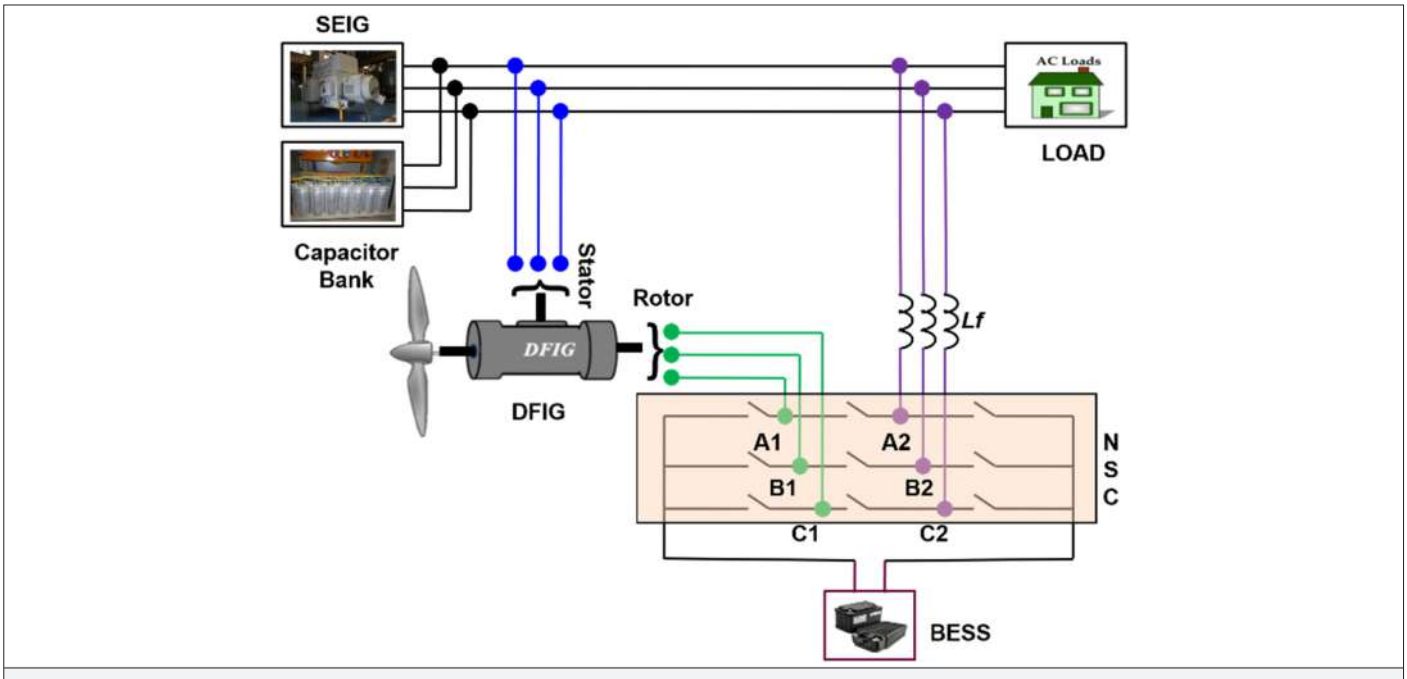

Fig. 1. Circuit diagram of a hybrid microgrid system.

III. CONTROL ALGORITHMS

A. Nine-Switch Converter Control

Both the rotor-side and grid-side power flow of the doubly fed induction generator in this HMS is solely supervised by an NSC, which helps in controlling the frequency and voltage to be balanced at constant values for different loading conditions. The terminals A_1, B_1, and C_1 of NSCs act as the rotor terminals of DFIG, whereas terminals A_2, B_2, and C_2 are connected across the SEIG terminals with the help of filter inductance (*Lf*) to control the voltage and frequency of the hybrid system. The stator-side power flow of the WECS is controlled by controlling the rotor currents of the DFIG through terminals A_1, B_1, and C_1 of NSCs. Similarly, "P" and "Q" compensation for HMS is controlled by I_c of A_2, B_2, and C_2 of NSCs. Both the power flow is independent of each other despite a single converter used for both operations. The control schemes and the structure of NSC are well studied in [14, 20].

B. Control Structure of Doubly Fed Induction Generator

Here, DFIG uses a direct vector control strategy that uses the quantities of stator terminal termed as SFOVC. In order to control both the real and reactive power of DFIG individually, two control loops are taken into consideration. Mainly, there are quadrature-axis (qA) loop and direct-axis (dA) loop. The qA loop inhibits speed errors $\left(\omega^* - \omega\right)$, which controls the real power. On the other hand, the dA loop either controls the machine flux or else controls the reactive power generated at the stators of DFIG. In order to enhance the dA loop, the reactive power element is set at zero (0), making the stator-side power factor operate at unity. Here, two conventional proportional integral controllers have been used, whose gains are obtained using a trial-and-error process to reach the near optimum results. Both dA and qA currents are estimated and converted to the three-phase reference frame. In order to obtain the control signals for terminal A_1, B_1, and C_1 of the NSC, the actual three-phase currents are compared with the reference three-phase currents, as shown in Fig. 2.

$$C_{A_1B_1C_1} = e_{A_1B_1C_1} = I_{r_{abc}}{}^{*} - I_{r_{abc}} \tag{1}$$

C. REAL-REACTIVE POWER COMPENSATION CONTROL ALGORITHM

The *NSC's* A_2, B_2, and C_2 terminals serve as the GSC of DFIG-based WECS. The A_2, B_2, and C_2 terminals are connected to the system through L_f . An NSC compensates the required real and reactive power to the system through the terminals A_2, B_2, and C_2. The compensating currents fed to the system through terminals A_2, B_2, *and* C_2 can be expressed as follows:

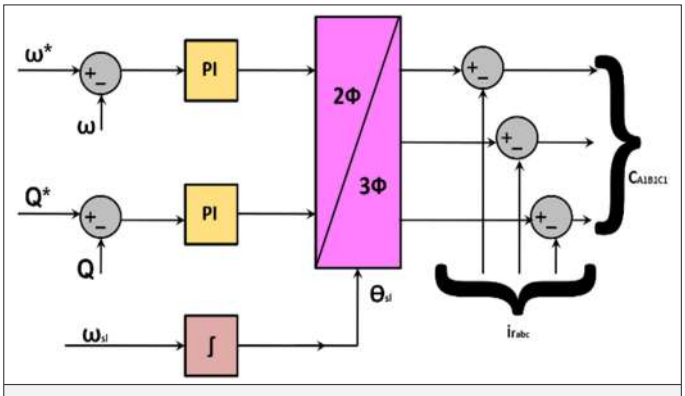

Fig. 2. Rotor-side control structure.

$$\frac{di_{cA_2B_2C_2}}{dt} = \frac{1}{L_f}\left(V_{s_{abc}} - V_{A_2B_2C_2} - R_f i_{cA_2B_2C_2}\right) \tag{2}$$

where $V_{s_{abc}}$ is the three-phase PCC voltage and $V_{A_2B_2C_2}$ is the voltage at terminal A_2, B_2, and C_2.

Again, equating the DC- and AC-side active power, we get

$$V_d I_d = P_{r_{abc}} + P_{A_2B_2C_2} \tag{3}$$

where $P_{r_{abc}}$ is the active power at A_1, B_1, and C_1 terminals of NSC and $P_{A_2B_2C_2}$ is the active power at the terminals A_2, B_2, and C_2 of NSC. Hence,

$$I_d = \frac{P_{r_{abc}} + P_{A_2B_2C_2}}{V_d} \tag{4}$$

From the battery model given in Fig. 3, the battery current can be expressed as discussed in [21] as follows:

$$I_b = \frac{V_d - E_b - V_{cb}}{R_{in}} \tag{5}$$

where

E_b is the battery voltage, V_{cb} is the voltage across capacitor, and R_{in} is the internal resistance of battery

Again,

$$\frac{dV_c}{dt} = \frac{1}{C_b}\left(I_b - \frac{V_{cb}}{R_b}\right) \tag{6}$$

From (4) and (5), the DC-link voltage V_d can be found as follows:

$$\frac{dV_c}{dt} = \frac{1}{C_d}\left(I_d - I_b\right) \tag{7}$$

Nine-switch converter terminals A_2, B_2, and C_2 take care of the real and reactive power compensation. When there is a power shortage, NSC stores the extra actual power in the BES for use. Additionally, the NSC compensates the system with enough reactive power to maintain a constant voltage profile despite load variations. Control systems for compensating real and reactive power are illustrated in Fig. 4.

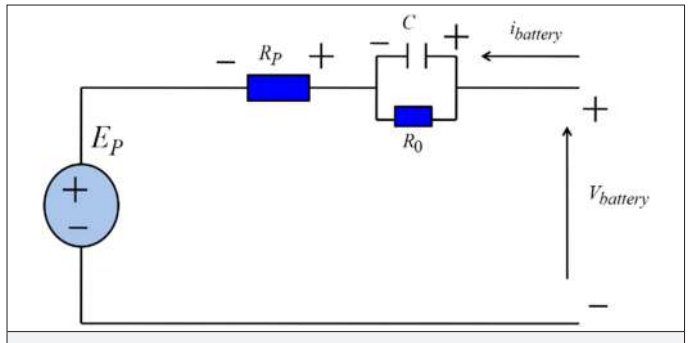

Fig. 3. Configuration of a battery energy storage.

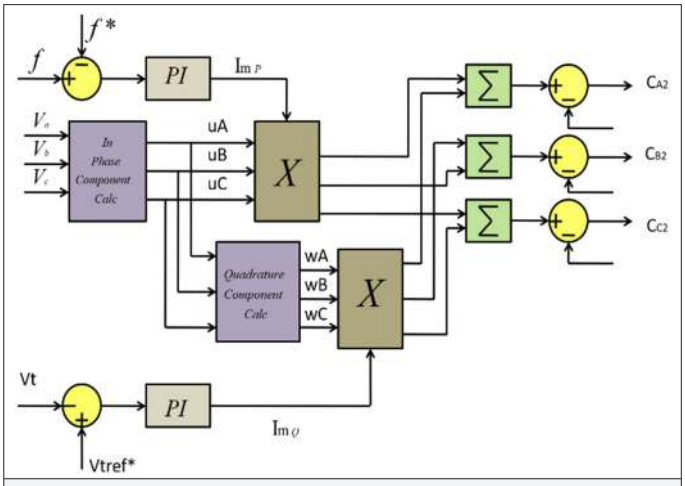

Fig. 4. Real-reactive power control algorithm.

The PCC voltages are sensed, and from the PCC voltages the peak voltage, in-phase voltage components, and quadrature voltage components are calculated as per (9) and (10), respectively.

$$V_m = \sqrt{\frac{2}{3}\left(V_a^2 + V_b^2 + V_c^2\right)} \tag{8}$$

$$u_a = \frac{V_a}{V_m}; u_b = \frac{V_b}{V_m}; u_c = \frac{V_c}{V_m} \tag{9}$$

$$\begin{bmatrix} w_a \\ w_b \\ w_c \end{bmatrix} = \begin{bmatrix} 0 & -\frac{1}{\sqrt{3}} & \frac{1}{\sqrt{3}} \\ \frac{\sqrt{3}}{2} & \frac{1}{2\sqrt{3}} & -\frac{1}{2\sqrt{3}} \\ -\frac{\sqrt{3}}{2} & \frac{1}{2\sqrt{3}} & -\frac{1}{2\sqrt{3}} \end{bmatrix} \begin{bmatrix} u_a \\ u_b \\ u_c \end{bmatrix} \tag{10}$$

The PI controller takes frequency error as input, which then calculates the magnitude of the reference in-phase current component I_P. Similarly, the magnitude of the reference quadrature current component I_Q is calculated from the PCC voltage error and is expressed as per (11) and (12).

$$I_{mP} = K_{p_P}(f - f^*) + K_{i_P}\int (f - f^*)dt \tag{11}$$

$$I_{mQ} = K_{p_Q}(Vt^* - Vt) + K_{i_Q}\int (Vt^* - Vt)dt \tag{12}$$

After the amplitudes are calculated, the reference in-phase and quadrature components of currents are determined as follows:

$$I_{Pabc} = I_{mP}{}^* u_{abc} \tag{13}$$

$$I_{Qabc} = I_{mQ}{}^* w_{abc} \tag{14}$$

The final three-phase reference currents are then found by adding the in-phase and quadrature components of the current

$$I_{cabc}{}^* = I_{Pabc} + I_{Qabc} \tag{15}$$

The actual compensation current I_{cabc} is then subtracted from the three-phase reference compensation currents $I_{cabc}{}^*$ to generate the control signals for the A_2, B_2, and C_2 terminals of the NSC.

$$C_{A_2B_2C_2} = e_{A_2B_2C_2} = I_{cabc}{}^* - I_{cabc} \tag{16}$$

The whole control structure is given in Fig. 4.

D. Generation of Switching Pulses for Nine-Switch Converter

The control signals "$C_{A_1B_1C_1}$" and "$C_{A_2B_2C_2}$" are given the required offset so that they do not intersect each other. The offset given to the control signals also decide the effective DC voltages which would be reflecting at the terminals A_1, B_1, and C_1 and A_2, B_2, and C_2. More offset, lesser will be the reflected DC voltage. Hence, the offsets are adjusted according to the DC-voltage requirement of terminals A_1, B_1, and C_1 and A_2, B_2, and C_2. In this work, total D-link voltage is determined to be 1800 V. The DC-voltage requirement for terminals A_1, B_1, and C_1 is less as compared to terminals A_2, B_2, and C_2. This is due to the fact that the rotor-side voltage is equal to the slip time of the

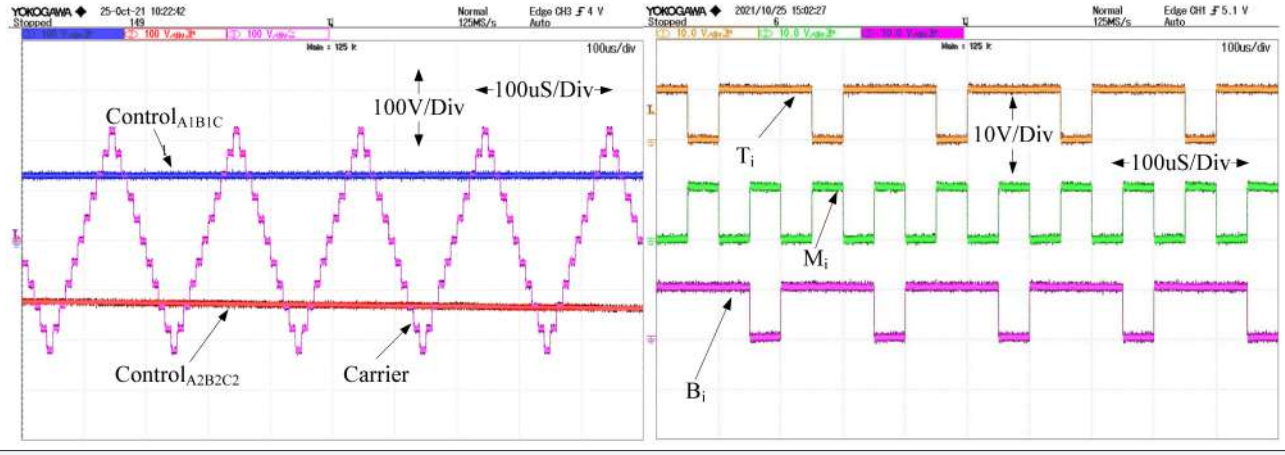

Fig. 5. Real-time representation of reference switching of a nine-switch converter.

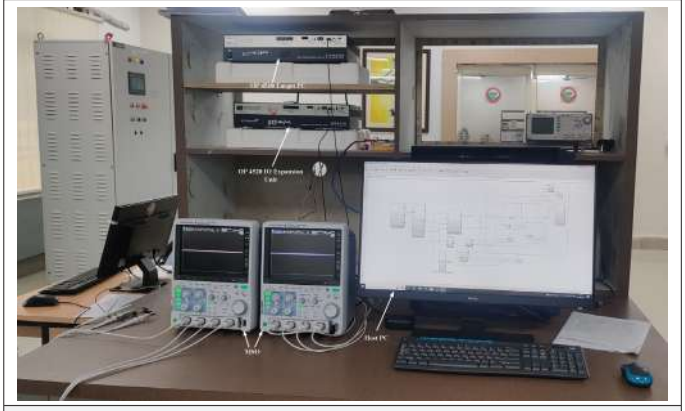

Fig. 6. Equivalent hardware setup for an isolated hybrid microgrid system.

stator-side voltage of the DFIG, due to which the DC-voltage requirement for terminals A_1, B_1, and C_1 would definitely be less as compared to terminals A_2, B_2, and C_2. Hence, the offset given to the control signal in this work is not equal. The offset is given such that the control signals "$e_{A_1}, e_{B_1}, e_{C_1}$" share 30% of the peak-to-peak values of the carrier, whereas the control signals "$e_{A_2}, e_{B_2}, e_{C_2}$" share 70% peak-to-peak value of the carrier wave. The reference switching signal is shown in Fig. 5.

IV. RESULT ANALYSIS

The NSC-established hybrid autonomous system is modeled, simulated, and verified using OPAL-RT in this section. The performance of the system is evaluated under different loads. The system is subjected to three distinct loads, i.e., base RL load, rectifier load, and induction motor load, and the results are analyzed to evaluate the performance and robustness of the system. The whole purpose of the NSC along with its control structure is to maintain constant frequency and voltage irrespective of load variation. The proposed work is verified on an OPAL-RT 4510 real-time digital simulator, which operates with the Kintex-7 FPGA platform. It comprises a parallel computing environment which provides a platform for obtaining some real-time outputs, and these outputs are equivalent to hardware results. The equivalent hardware setup is shown in Fig. 6. The detailed configuration of this hardware setup is given in Table I. The proposed isolated HMS is first developed and simulated using MATLAB/Simulink environment directly via RT-Lab. For obtaining results and figures, two Mixed Signal Oscilloscope (MSO) of four channels each were used, which are configured as YOKOGAWA DLM 3024, 2.5 GS/s 200 MHz.

TABLE I. REAL-TIME SIMULATION PARAMETERS

Parameters	Specifications
Type of simulation	Real time
Step time	μs
Operating system	Windows 10
Simulator	OP 4510 (RCP/HIL Kintex-7 FPGA Processor)
Memory	32 GB
FPGA software	Xilinx Kintex-7 FPGA, 485T
Target software used	RT-Lab

A. Performance Analysis of the Proposed System with Time-Varying RL Load

This section presents the currents and voltages of the proposed system when subjected to linear RL load. Initially, the load is reduced from 3.8 kW to 1.04 kW, and step increase in load can be observed from 3.8 kW to 5.6 kW. Accordingly, the compensation current (I_C) suggests the appropriate behavior of the load change, as can be seen from Fig. 7. This compensation current helps in managing the real and reactive power of the system, which furthermore helps in maintaining the system frequency and voltage to be constant. During the reduction in load, the excess power is stored in BES, whereas during increase in load the deficit power is extracted from BES to the system. From Fig. 8, it can be seen that the DC-link current accordingly decreases, when there is a power requirement in the system. Moreover, the SEIG and DFIG voltage and currents remain approximately constant throughout the system irrespective of any load variation. The frequency of the system remains steady throughout.

B. Performance Analysis of the Proposed System During Rectifier Load Switching

Here, the non-linear load considered is a three-phase full-bridge diode rectifier with RL load. Initially, the power is fed to a linear RL load, and the rectifier load is switched on at a specific time interval which causes the load current to be distorted. From the load current (Fig. 9), it can be seen that the distortion in the sinusoidal wave is non-linear in nature.

Switching of the rectifier load helps in injecting a very high value of harmonics into the system current, which needs to be filtered out for efficient performance of the system. The terminal A_2, B_2, and C_2 of NSC acts as a shunt active filter to mitigate the injected harmonics by the rectifier load, whereas the terminals A_1, B_1, and C_1 help in controlling the stator-side power flow of the DFIG. Moreover, NSC acts as both a shunt active filter and a static synchronous generator. The operation of the NSC as active filter helps to reduce the harmonics in the system current, whereas it also acts as SSG to compensate the required real and reactive power of the system so as to maintain the frequency and voltage to be constant throughout the system. Fig. 10 shows the battery current which is being fed to the system to match the real power demand during rectifier load switching. The frequency of the system remains constant. Fig. 11 shows the THD analysis of the generator current and load current.

C. Performance Analysis of the Proposed System During Induction Motor Load Switching

The system is initially subjected to a linear RL load, and at a specific time interval the induction motor load is started direct online (DOL). The real and reactive power demand is too high as induction motor draws high starting current, as can be seen in Fig. 12. This implies the sudden decrease in the voltage at the DC side, which is nearly around 20 V as can be seen from Fig. 13. The reduction in DC-link voltage causes the BES to discharge and supply power to the system in order to stabilize frequency and voltage of the system. The voltage and current of SEIG and DFIG remain unchanged

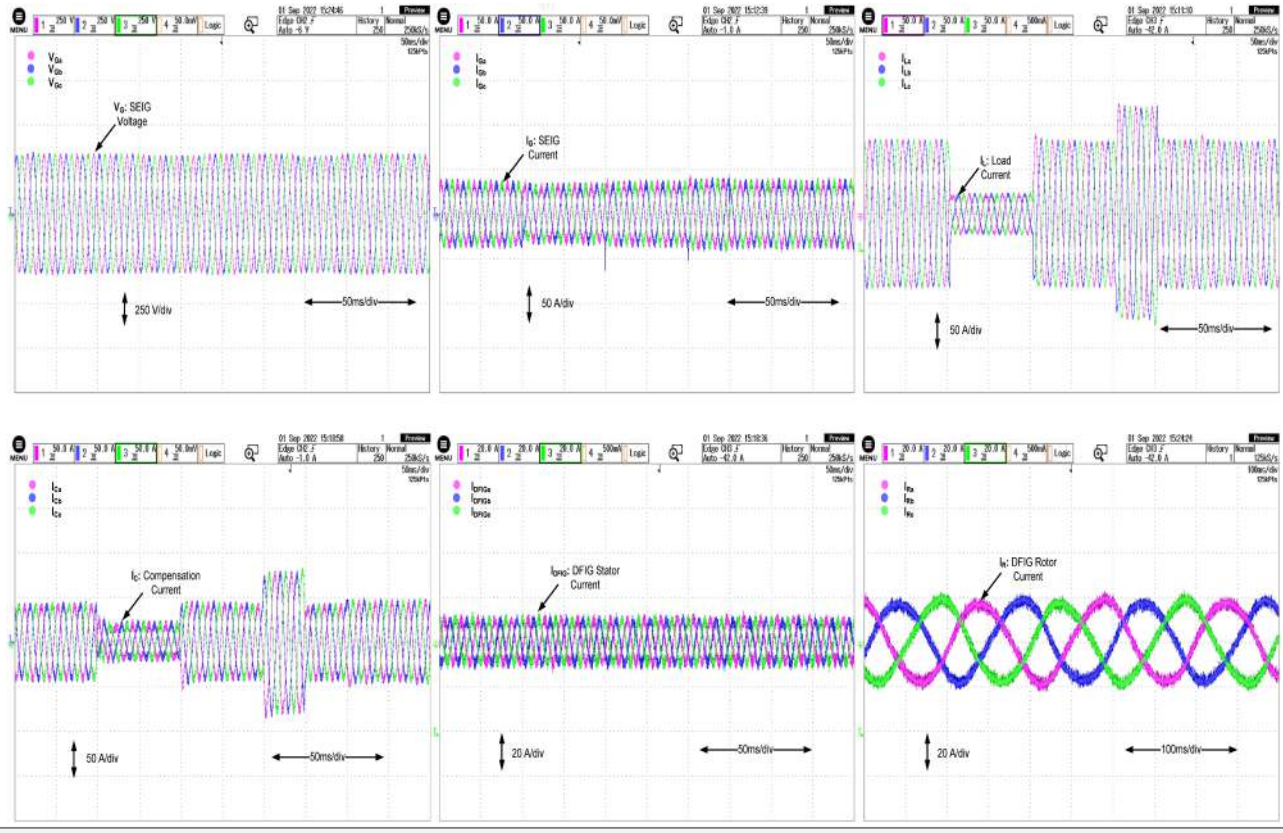

Fig. 7. Real-time validation of the proposed system: AC voltage and currents during linear load change.

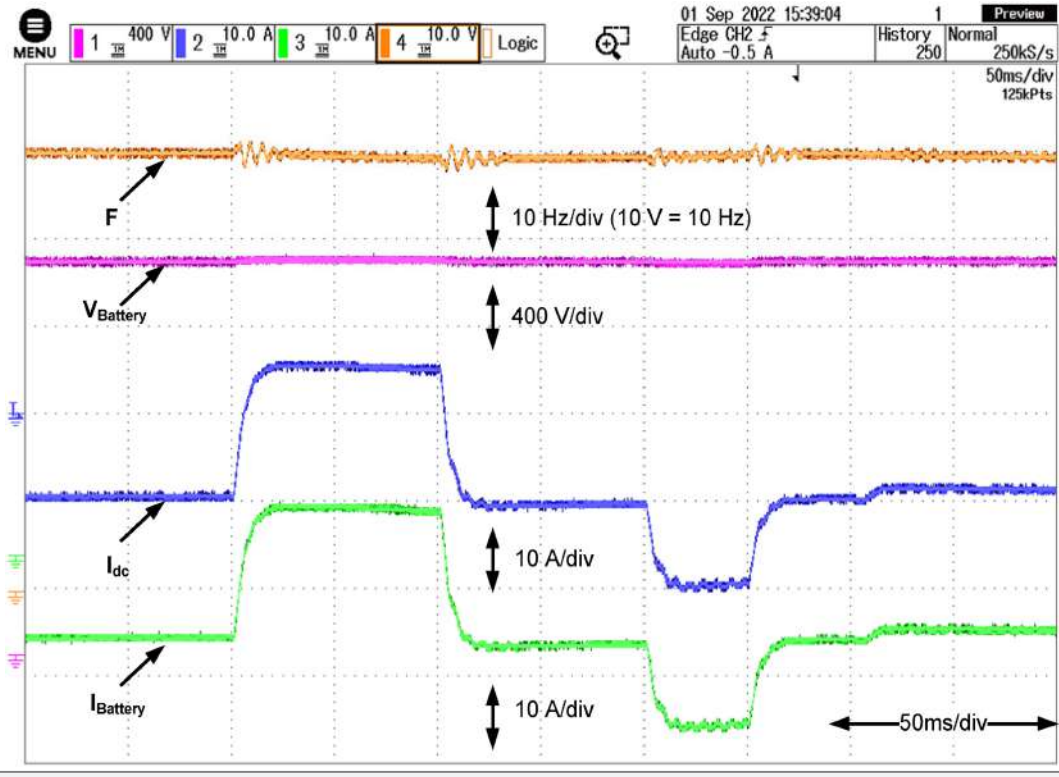

Fig. 8. Real-time validation of the proposed system: DC voltage and currents during linear load change.

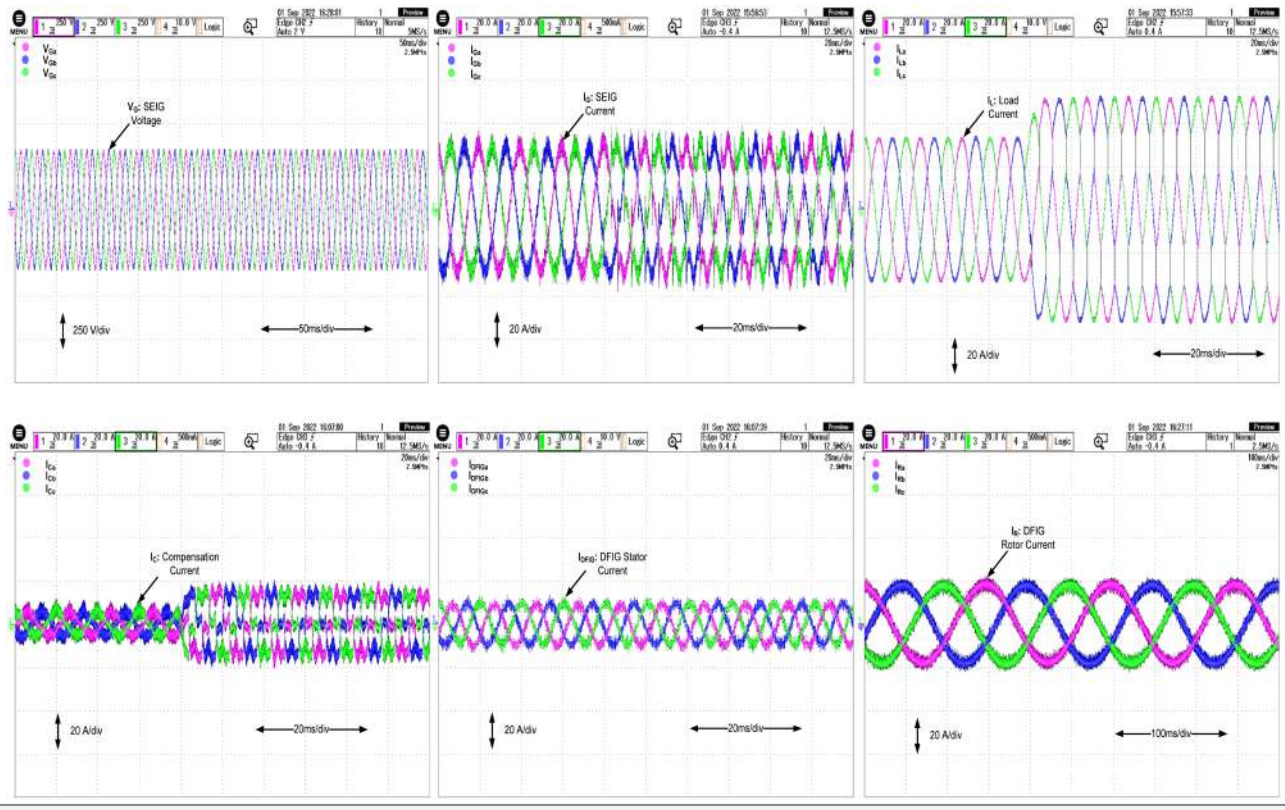

Fig. 9. Real-time validation of the proposed system: AC voltage and currents during rectifier load switching.

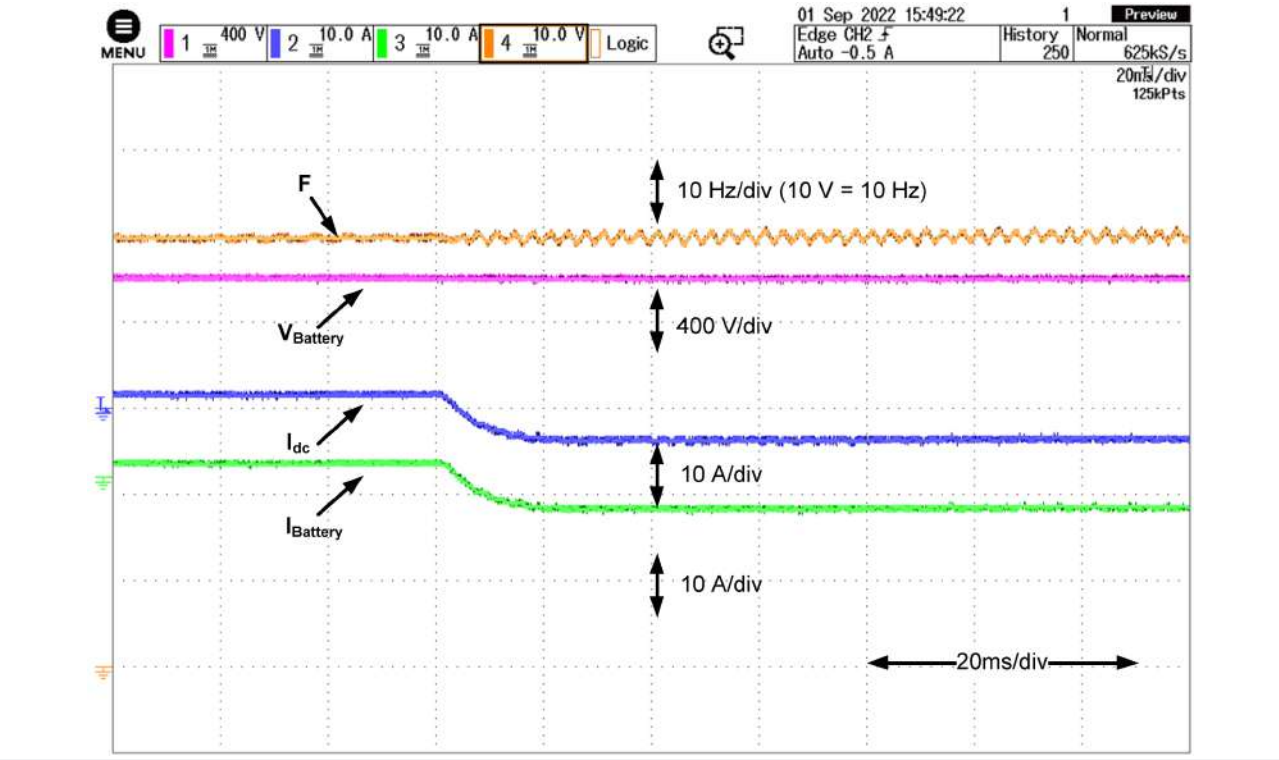

Fig. 10. Real-time validation of the proposed system: DC voltage and currents during rectifier load switching.

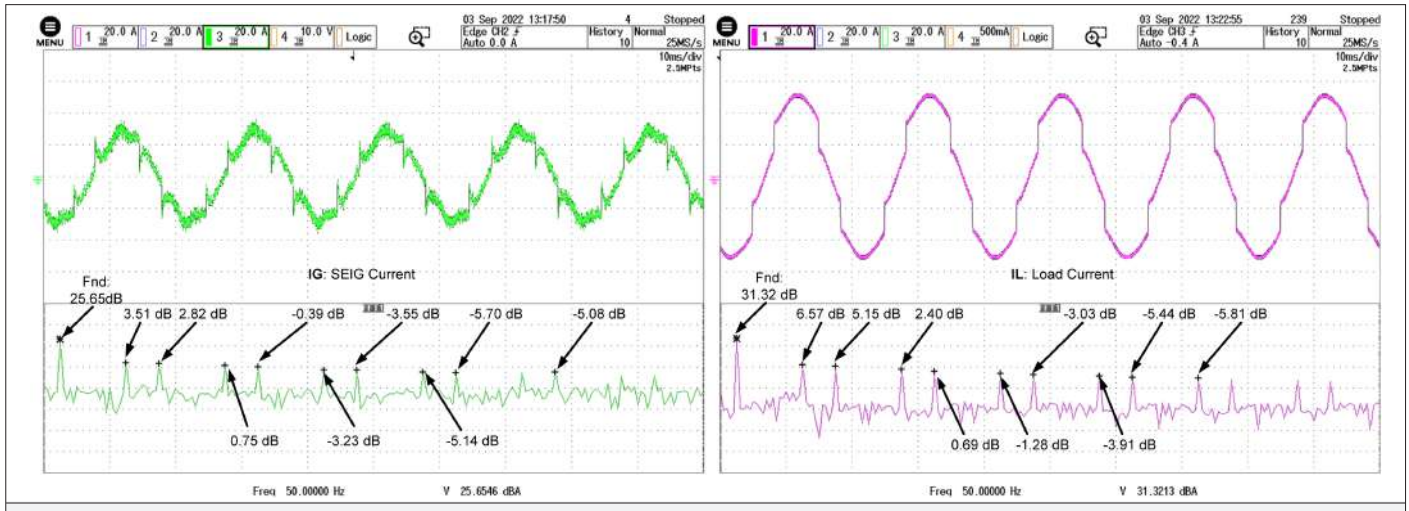

Fig. 11. Fast Fourier transforms (FFT) analysis of generator and load currents during rectifier load switching.

irrespective of induction motor load switching which is dynamic in nature.

The NSC also acts as a STATCOM to compensate the reactive power demand of the load which helps in stabilizing the voltage profile of the system. The battery current and frequency waveforms can be seen from Fig. 13.

D. Performance With Step Change in SEIG and DFIG Torques

In this section, a linear load that is assumed to be constant is powered by the system. The turbine torques of SEIG and DFIG are altered in steps. If not addressed, the fluctuating turbine torques will affect the SEIG and DFIG currents. That might lead to changes in system voltage and frequency. As can be observed from Figs 14 and 15, the NSC in this situation balances power so well that the system voltage

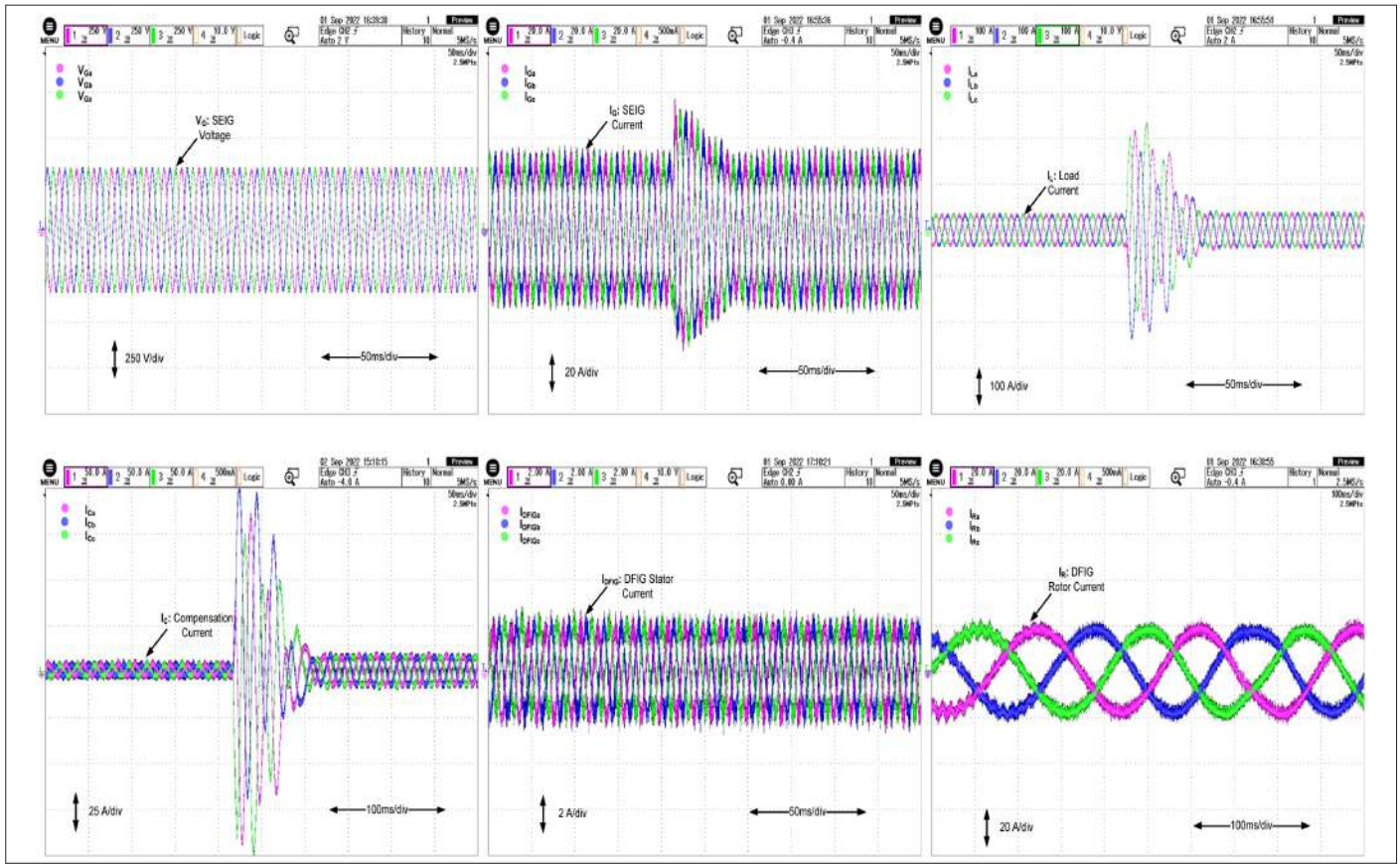

Fig. 12. Real-time validation of the proposed system: AC voltage and currents during induction motor load switching.

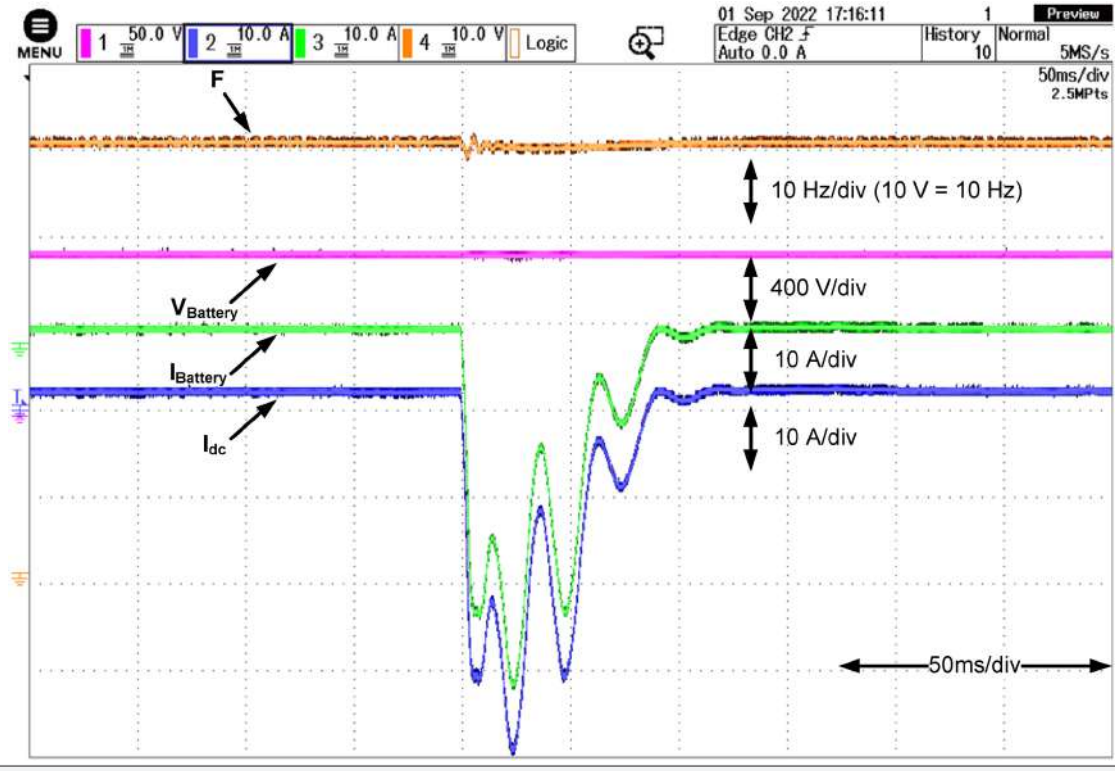

Fig. 13. Real-time validation of the proposed system: DC voltage and currents during induction motor load switching.

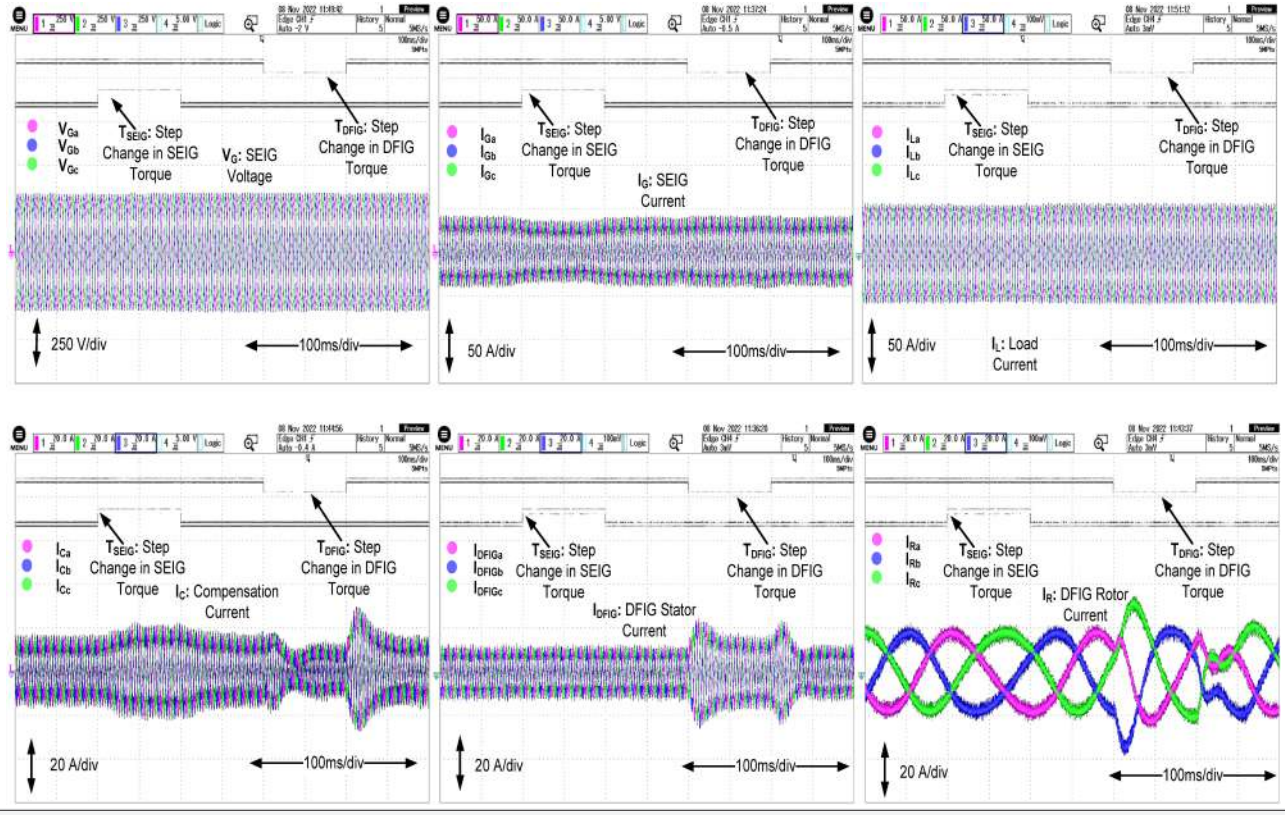

Fig. 14. Real-time validation of the proposed system: AC voltage and currents during step change in SEIG and DFIG torques.

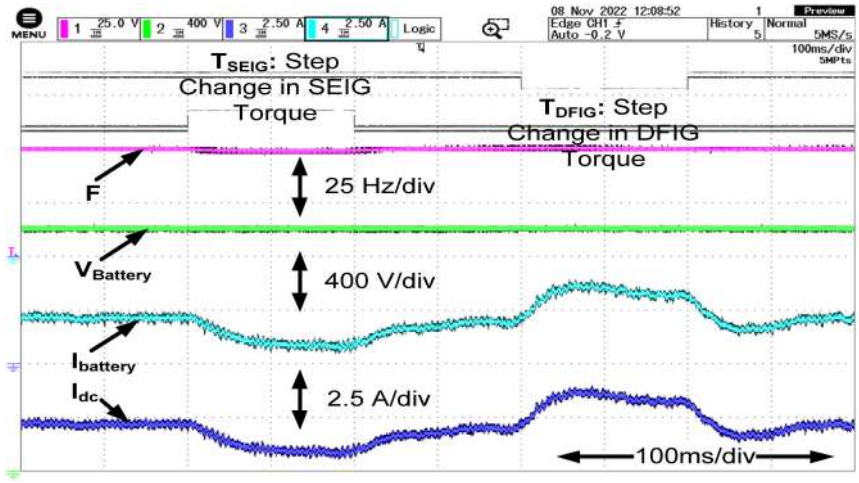

Fig. 15. Real-time validation of the proposed system: DC voltage and currents during step change in SEIG and DFIG torques.

and frequency stay constant. The SEIG torque is reduced from –85 Nm to –75 Nm, whereas the DFIG torque is increased from –25 Nm to –35 Nm at different intervals. It can be noted that the compensation current varies according to the torque variation to maintain a constant frequency and voltage in the system. In order to store or supply surplus or deficit active power to the system and keep the system frequency constant, the NSC efficiently modulates the DC-link voltage, as shown in Fig. 15.

V. CONCLUSION

In hybrid autonomous systems, BTB converters are frequently utilized for power management control and interface. Due to the availability of the DC link, these converters in particular offer a wide range of applications for managing the power separately. The BTB converters have been reconfigured with NSCs in this operation. Here, NSC is used to incorporate renewable energy sources, and the system's power management is assessed. The hybrid system comprises NSCs that interconnect SEIG and DFIG. The NSC functions as the SSG to control the system's real and reactive power as well as a shunt active filter to remove harmonics from the system. During any load problems, the voltage and current on the generator side and the side of the wind turbine largely remain unchanged. As a result, it was determined that the control structure created for real and reactive power adjustment as well as RSC control is effective. "0" overruns were found during the system's OPAL-RT 4510 verification, indicating that the system was validated in real time.

Peer-review: Externally peer-reviewed.

Author Contributions: Concept – A.C., S.P.; Design – A.C., S.P.; Supervision – R.S., S.K.K.; Literature Review – A.C.; Writing – A.C.; Critical Review – S.P.

Declaration of Interests: The authors have no conflicts of interest to declare.

Funding: The authors declared that this study has received no financial support.

REFERENCES

1. R. Pena, J. C. Clare, and G. M. Asher, "Doubly fed induction generator using back-to-back PWM converters and its application to variable-speed wind-energy generation," *IEE Proc. Electr. Power Appl.*, vol. 143, no. 3, pp.231–241, 1996. [CrossRef]
2. A. Mohanty, S. Patra, and P. K. Ray, "Robust fuzzy-sliding mode based UPFC controller for transient stability analysis in autonomous wind-diesel-PV hybrid system," *IET Gener. Transm. Distrib.*, vol. 10, no. 5, pp.1248–1257, 2016. [CrossRef]
3. A. S. Lunardi, J. S. Chaves, and A. J. Sguarezi Filho, "Predictive direct torque control for a squirrel cage induction generator grid connected for wind energy applications," *IEEE Lat. Am. Trans.*, vol. 14, no. 11, pp.4454–4461, 2016. [CrossRef]
4. S. Pati, K. B. Mohanty, and S. K. Kar, "A sliding mode controller-based STATCOM for voltage profile improvement of micro-grids," *World J. Eng.*, vol. 15, no. 2, 283–291, 2018. [CrossRef]
5. S. Pati, K. B. Mohanty, A. Choudhury, and S. Kar, "Integration and power control of a micro-hydro-PV-wind based hybrid microgrid," In 2017 International Conference on Circuit, Power and Computing Technologies (ICCPCT). IEEE Publications, 2017, pp. 1–6. [CrossRef]
6. S. Shao, E. Abdi, F. Barati, and R. McMahon, "Stator-flux-oriented vector control for brushless doubly fed induction generator," *IEEE Trans. Ind. Electron.*, vol. 56, no. 10, pp.4220–4228, 2009. [CrossRef]
7. I. Villanueva, A. Rosales, P. Ponce, and A. Molina, "Grid-voltage-oriented sliding mode control for DFIG under balanced and unbalanced grid faults," *IEEE Trans. Sustain. Energy*, vol. 9, no. 3, pp.1090–1098, 2017. [CrossRef]
8. Y. Pang *et al.*, "Model predictive control of nine-switch converter with output filter for independent control of two loads," *J. Power Electron.*, vol. 21, no. 1, pp.224–234, 2021. [CrossRef]
9. S. Datta, J. P. Mishra, and A. K. Roy, "Operation and control of a DFIG-based grid-connected WECS using NSC during grid fault and with unbalanced non-linear load," *Int. J. Ambient Energy*, vol. 39, no. 7, pp.732–742, 2018. [CrossRef]
10. A. Kirakosyan, M. S. El Moursi, P. Kanjiya, and V. Khadkikar, "A nine switch converter-based fault ride through topology for wind turbine applications," *IEEE Trans. Power Deliv.*, vol. 31, no. 4, pp.1757–1766, 2016. [CrossRef]
11. F. Gao, L. Zhang, D. Li, P. C. Loh, Y. Tang, and H. Gao, "Optimal pulsewidth modulation of nine-switch converter," *IEEE Trans. Power Electron.*, vol. 25, no. 9, pp.2331–2343, 2010. [CrossRef]
12. R. Majumder, A. Ghosh, G. Ledwich, and F. Zare, "Power management and power flow control with back-to-back converters in a utility connected microgrid," *IEEE Trans. Power Syst.*, vol. 25, no. 2, pp. 821–834, 2009. [CrossRef]
13. F. Gao, H. Tian, and N. Li, "Dead-time elimination method of nine-switch converter," *IET Power Electron.*, vol. 7, no. 7, pp.1759–1769, 2014. [CrossRef]
14. A. Choudhury, S. Mohanty, S. Pati, S. K. Kar, S. K. Mahalik, and R. K. Swain, "Integration and Control of a Hybrid Isolated System using SMC based nine Switch Converter," In 2020 IEEE 9th Power India International Conference (PIICON). IEEE Publications, 2020, pp. 1–6. [CrossRef]
15. A. Choudhury, S. Pati, S. K. Kumar Kar, and R. Sharma, "Hybridization and power control of an isolated PV-SEIG-based generation System using novel nine Switch converter, " *Electrica*. [CrossRef]

16. A. Choudhury, S. Khatua, S. Pati, and S. K. Kar, "A reliable and efficient integration topology for autonomous hybrid systems using NSC," In 2019 International Conference on Electrical, Electronics and Computer Engineering (UPCON). IEEE Publications, 2019, pp. 1–6. [CrossRef]
17. B. Singh, S. S. Murthy, and S. Gupta, "Analysis and design of STATCOM-based voltage regulator for self-excited induction generators," *IEEE Trans. Energy Convers.*, vol. 19, no. 4, pp.783–790, 2004. [CrossRef]
18. B. Singh, and S. Sharma, "Doubly fed induction generator-based off-grid wind energy conversion systems feeding dynamic loads," *IET Power Electron.*, vol. 6, no. 9, pp.1917–1926, 2013. [CrossRef]
19. S. Pati, K. B. Mohanty, and S. K. Kar, "Performance improvement of a STATCOM using fuzzy controller for isolated generator," *World J. Eng.*, vol. 15, no. 2, 273–282, 2018. [CrossRef]
20. A. Choudhury, S. Mohanty, S. Pati, S. K. Kar, and R. K. Swain, "A Mamdani-FLC based nine Switch Converter Topology for Integration and Power Control of HAS," In 2020 International Conference on Computational Intelligence for Smart Power System and Sustainable Energy (CISPSSE). IEEE Publications, 2020, pp. 1–6. [CrossRef]
21. C. -J. Zhan *et al.*, "Two electrical models of the lead–acid battery used in a dynamic voltage restorer," *IEE Proc. Gener. Transm. Distrib.*, vol. 150, no. 2, pp.175–182, 2003. [CrossRef]

Abhijeet Choudhury completed his Bachelor of Technology from ITER, SOAU, Bhubaneswar. He completed his Masters of Technology in Power Electronics and Drives from Department of Electrical Engineering, ITER, SOAU, Bhubaneswar. He is currently pursuing his PhD at Siksha O Anusandhan Deemed to be University in the Department of Electrical Engineering. He is currently working as a Faculty in Department of Electrical Engineering at SOADU, Bhubaneswar. His research area includes AC/DC Microgrid, Electrical Machine & Drives, Integration and Power management of Hybrid autonomous system, Design of different converter topology, Renewable Energy etc.

Dr. Swagat Pati completed his Bachelor of Technology from ITER, Bhubaneswar. He completed his Masters of Research in Power Electronics and Drives from NIT, Rourkela. He was awarded his PhD from Siksha O Anusandhan Deemed to be University. Presently he is working as Assistant Professor in Department of Electrical Engineering, ITER, Siksha O Anusandhan Deemed to be University. His research area includes Integration and Power control of Hybrid Renewable energy systems, design of new topology for power electronic converters, electric drives application, FACTS devices.

Dr. Sanjeeb Kumar Kar completed his Bachelor of Technology from College of Engineering and Technology, Bhubaneswar. He completed his Masters of Technology and PhD from IIT, Kharagpur from the Department of Electrical Engineering in Control Systems. Presently he is working as Professor in the Department of Electrical Engineering, ITER, Siksha O Anusandhan Deemed to be University. His research area includes Control System, Power System Optimisation, AGC, Integration and Power management. He has already guided more than a dozens of PhD in his career.

Renu Sharma works as a Professor in the Department of Electrical Engineering at Siksha 'O 'Anusandhan Deemed to be University, Bhubaneswar, India. She is Senior Member IEEE, Life Member IE (India), Member of IET, Life member ISTE, Life member ISSE, Past Chair WIE IEEE Bhubaneswar Sub Section. Her research areas are Smart Grid, Soft Computing, Solar Photovoltaic systems, Power System Scheduling, Evolutionary Algorithms and Wireless Sensor Networks. She has published around 100 journal and conference articles of International Repute. She has organized several national and international conferences. She is guest editor of Special Issue in International Journal of Power Electronics, Inderscience. Also, Guest Editor of Special Issue in International Journal of Innovative Computing and Applications, Inderscience. She has coordinated AICTE sponsored FDP programs. She was one of the Plenary Chair PEDES 2020. She has around 21 years of leading impactful Technical, Professional, Educational experience. She was General Chair IEEE ODICON 2021, flagship conference IEEE WIECON-ECE 2020, Springer conference GTSCS-2020, IEPCCT-2019, IEPCCT 2021. She is serving publication Chair INDISCON-2022.